Expanded View Figures

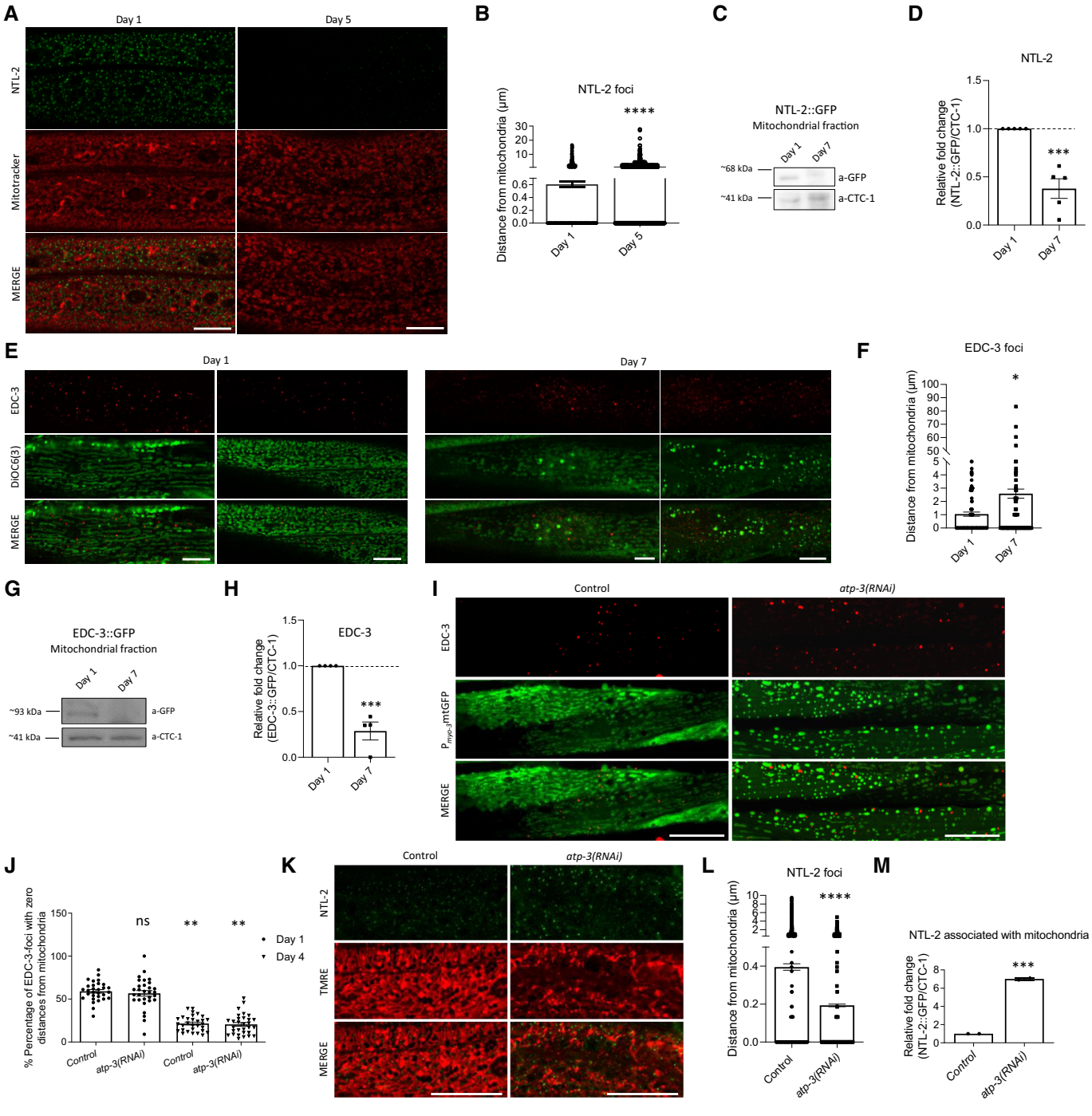

Figure EV1.

© 2023 The Authors

Figure EV1. The association of CCR4-NOT and mRNA degradation complex components with mitochondria is age-dependent.

A Representative images showing the localization of NTL-2 foci relative to mitochondria in young versus old animals (green: NTL-2, red: Mitotracker Deep Red FM, a mitochondrial-specific dye; $n = 2$ independent experiments).
B Quantification of the distances, the NTL-2 foci obtain from mitochondria in young versus older animals ($n = 3$ independent experiments with at least 40 animals/experiment; $^{****}P < 0.0001$; two-tailed unpaired *t*-test).
C Representative image from immunoblot analysis showing that NTL-2–mitochondria association decreases during ageing.
D Respective quantification ($n = 5$ independent experiments, $^{***}P < 0.001$; two-tailed unpaired *t*-test).
E Representative images showing the localization of EDC-3 foci relative to mitochondria in young (left) versus old animals (right) (red: EDC-3, green: DiOC6(3)) ((3,3′-dihexyloxacarbocyanine Iodide), a mitochondrial-specific dye; $n = 2$ independent experiments; image of day 1 adults in left is reused in Fig EV2K as conditions shown in (E) and Fig EV2K are part of the same experimental setup).
F Quantification of the distances EDC-3 foci obtain from mitochondria in young versus older animals ($n = 2$ independent experiments with at least 40 animals/experiment; $^{*}P < 0.05$; two-tailed unpaired *t*-test).
G Representative image from immunoblot analysis showing that EDC-3 is less associated with mitochondria in older animals compared to younger ones.
H Respective quantification ($n = 4$ independent experiments; $^{***}P < 0.001$; two-tailed unpaired *t*-test).
I Representative images showing the localization of EDC-3 foci relative to mitochondria in young adult animals upon genetic inhibition of *atp-3* (red: EDC-3, green: mitochondrial matrix targeted by GFP; $n = 2$ independent experiments).
J Quantification of the percentage of EDC-3 foci with zero distance from mitochondria under control conditions and following genetic inhibition of *atp-3* at days 1 and 4 of adulthood ($n = 2$ independent experiments with at least 40 animals/experiment; $^{**}P < 0.01$; one-way analysis of variance (ANOVA)).
K Representative images showing the localization of NTL-2 foci relative to mitochondria in control conditions and upon genetic inhibition of *atp-3* (green: NTL-2, red: TMRE, a mitochondrial membrane potential-dependent dye; $n = 2$ independent experiments).
L Quantification of the distances of NTL-2 foci from mitochondria in control conditions and upon genetic inhibition of *atp-3* ($n = 2$ independent experiments with at least 30 animals/experiment; $^{**}P < 0.01$; two-tailed unpaired *t*-test).
M Quantification of the NTL-2 protein bound to mitochondria under control conditions and upon genetic inhibition of *atp-3* (immunoblot analysis is shown in Fig 5E, $n = 2$ independent experiments; $^{**}P < 0.01$; unpaired two-tailed *t*-test).

Data information: Images were acquired using an ×63 objective lens. Scale bars, 20 μm. Error bars denote SEM.

© 2023 The Authors

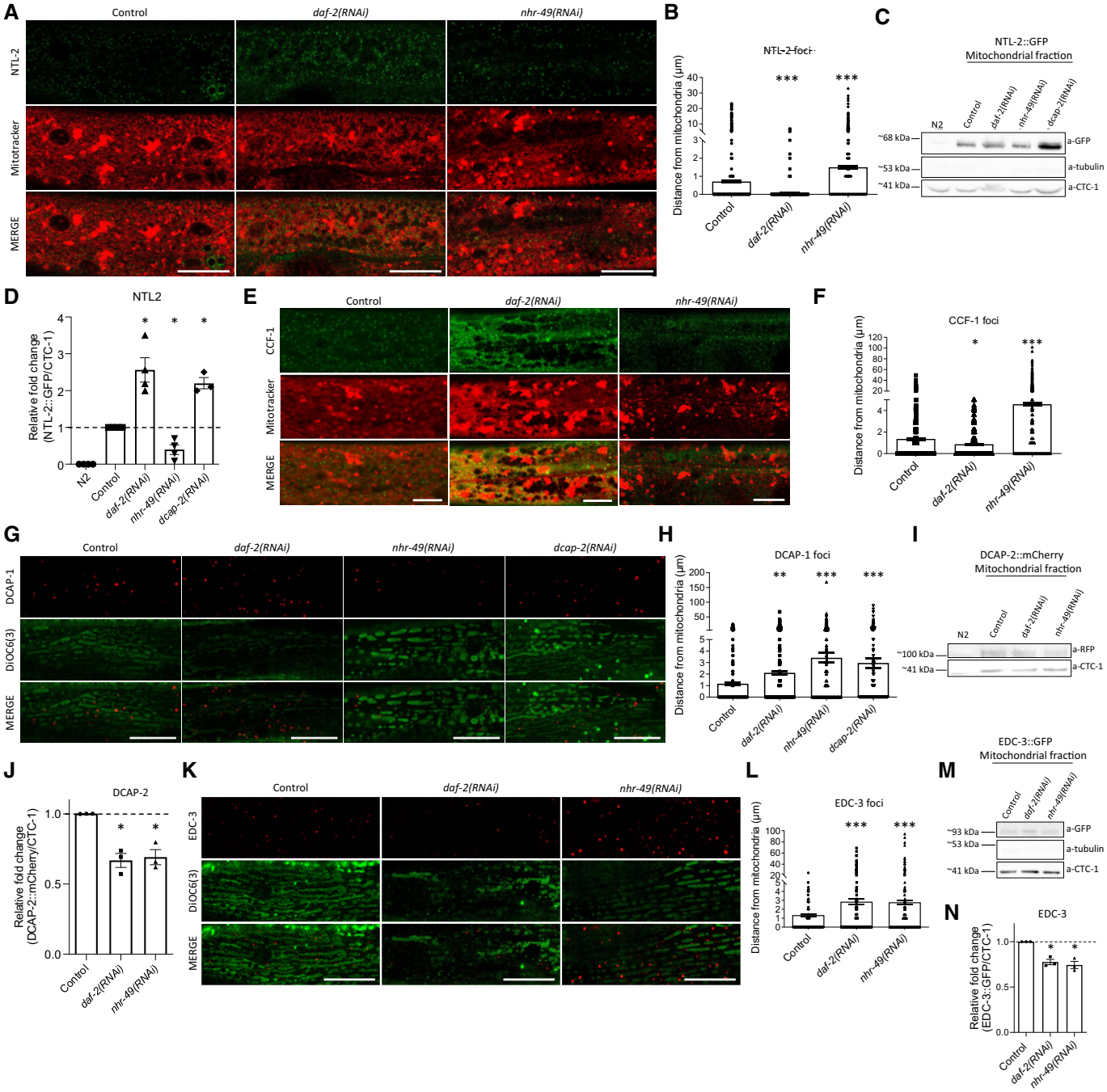

Figure EV2.

© 2023 The Authors

Figure EV2. Association of the CCR4-NOT and the mRNA degradation complex components with mitochondria is tightly and differentially regulated in long- and short-lived animals.

A Representative images showing the localization of NTL-2 foci relative to mitochondria upon genetic inhibition of either *daf-2* known to extend lifespan or *nhr-49* known to shorten lifespan (green: NTL-2, red: Mitotracker Deep Red FM, a mitochondria-specific dye).

B Quantification of the distances NTL-2 foci obtain from mitochondria upon genetic inhibition of *daf-2* or *nhr-49* (n = 3 independent experiments with at least 45 animals/experiment; ***P < 0.001; one-way analysis of variance (ANOVA)).

C Immunoblot analysis in isolated mitochondria of 1-day-old animals showing the protein levels of NTL-2 present in the mitochondrial isolate derived from animals under control conditions and upon the indicated genetic inhibitions.

D Quantification of western blot presented in B (n = at least 3 independent experiments; *P < 0.05; Welch's one-way analysis of variance (ANOVA) followed by Dunnett's T3 multiple-comparisons test).

E Representative images showing the localization of CCF-1 foci relative to mitochondria upon genetic inhibition of *daf-2* or *nhr-49* in day 1 adults; image in control is reused in Appendix Fig S3A as conditions shown in Appendix Fig S3A and (E) are part of the same experimental setup (green: CCF-1, red: Mitotracker Deep Red FM, a mitochondrial-specific dye).

F Quantification of the distances CCF-1 foci obtain from mitochondria upon genetic inhibition of *daf-2* or *nhr-49* (n = 3 independent experiments with at least 45 animals/experiment; *P < 0.05, ***P < 0.001; one-way analysis of variance (ANOVA)).

G Representative images showing the localization of DCAP-1 foci relative to mitochondria upon genetic inhibition of *daf-2*, *nhr-49* or *dcap-2* (red: DCAP-1, green: DiOC6 (3), a mitochondria-specific dye).

H Quantification of the distances DCAP-1 foci obtain from mitochondria upon genetic inhibition of *daf-2*, *nhr-49* or *dcap-2* (n = 3 independent experiments with at least 45 animals/experiment; **P < 0.01, ***P < 0.001; one-way analysis of variance (ANOVA)).

I Immunoblot analysis in isolated mitochondria of 1-day-old animals showing the protein levels of DCAP-2 present in the mitochondrial isolate in control conditions and upon the indicated genetic inhibitions.

J Respective quantifications (n = at least 3 independent experiments; *P < 0.05; Welch's one-way analysis of variance (ANOVA) followed by Dunnett's T3 multiple-comparisons test).

K Representative images showing the localization of EDC-3 foci relative to mitochondria upon genetic inhibition of *daf-2* or *nhr-49* in day 1 adults (red: EDC-3, green: DiOC6(3), a mitochondria-specific dye; image in control is reused in Fig EV1E as conditions shown in Figs EV1E and (K) are part of the same experimental setup).

L Quantification of the distances EDC-3 foci (shown in dots) obtain from mitochondria upon genetic inhibition of *daf-2* or *nhr-49* (n = 3 independent experiments with at least 45 animals/experiment; ***P < 0.001; one-way analysis of variance (ANOVA)).

M Immunoblot analysis in isolated mitochondria of 1-day-old animals showing the protein levels of EDC-3 present on mitochondria in control conditions and upon the indicated genetic inhibitions.

N Respective quantification (n = 3 independent experiments; *P < 0.05; Welch's one-way analysis of variance (ANOVA) followed by Dunnett's T3 multiple-comparisons test).

Data information: Images were acquired using a ×63 objective lens. Scale bars, 20 μm. Error bars denote SEM.

© 2023 The Authors

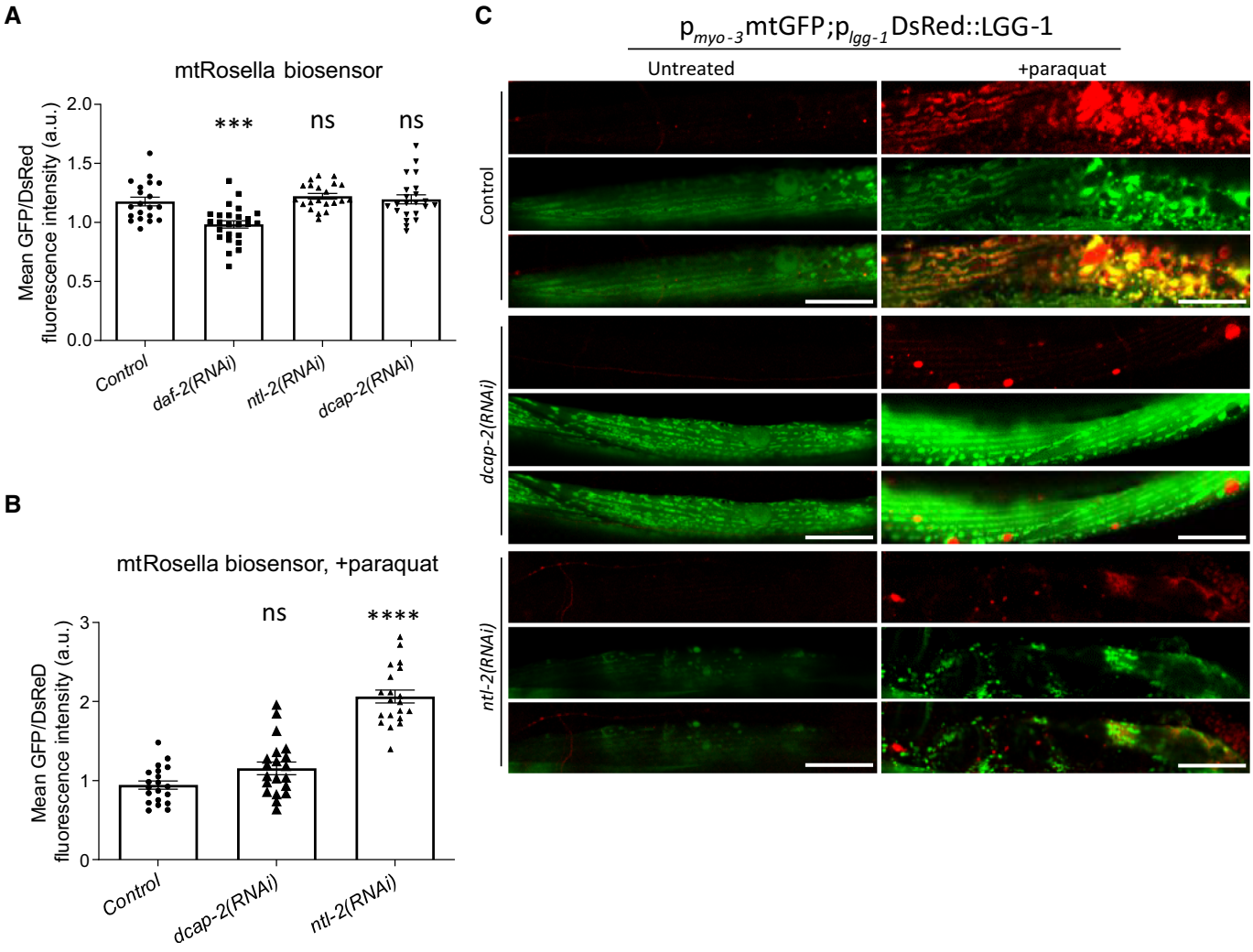

Figure EV3. Perturbation of CCR4-NOT and mRNA degradation complex components blocks mitophagy induction.

A, B Transgenic animals expressing the mitochondria-targeted Rosella (mtRosella) biosensor in body wall muscles were used to assess mitophagy (A) upon genetic inhibition of either *ntl-2* or *dcap-2* under control conditions; *daf-2* RNAi is used as a positive control ($n = 3$ independent experiments with at least 88 animals/experiment; ***$P < 0.001$; one-way analysis of variance (ANOVA)) and (B) after paraquat treatment ($n = 2$ independent experiments with at least 30 animals/experiment; ****$P < 0.0001$; one-way analysis of variance (ANOVA)). Mitophagy induction is signified by the reduction in the ratio between pH-sensitive GFP to pH-insensitive DsRed.

C Representative images showing mitophagy events under control conditions and following paraquat treatment in animals expressing a mitochondria-targeted GFP, together with the autophagosomal marker LGG-1 fused with DsRed in body wall muscle cells and subjected to either *dcap-2* or *ntl-2* RNAi (green: mitochondria, red: autophagosomes; yellow: mitophagy events; $n = 2$ independent experiments).

Data information: Images were acquired using an ×40 objective lens. Scale bars, 20 μm. Error bars denote SEM.

© 2023 The Authors

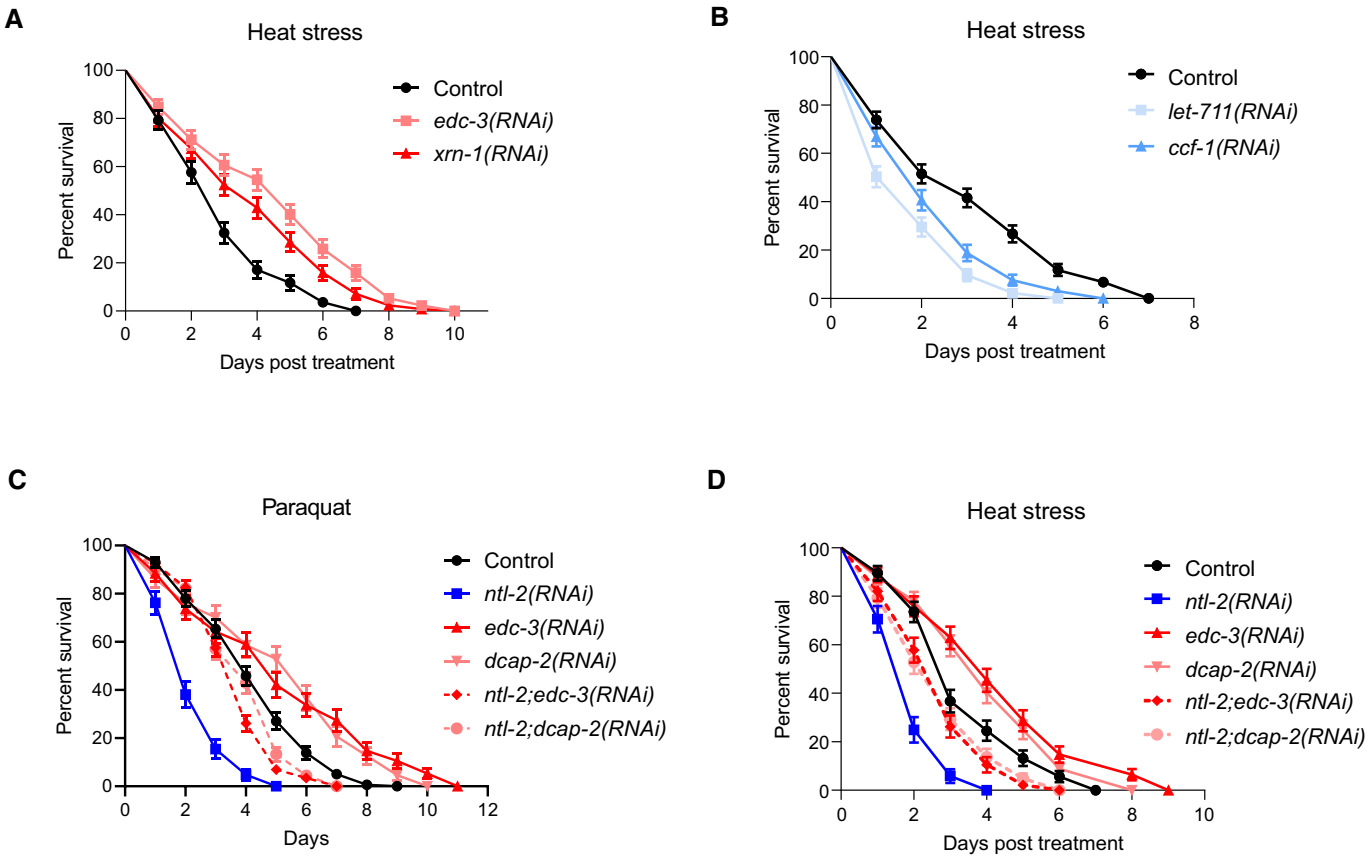

Figure EV4. Balance between storage and degradation body components is indispensable for animal stress resistance.

A Per cent survival of wild-type, EDC-3- and XRN-1-depleted animals exposed to heat stress for 5 h at 37°C and then counted every 24 h (n = 3 independent experiments with at least 369 animals/experiment).

B Per cent survival of wild-type, LET-711- and CCF-1-depleted animals exposed to heat stress performed for 5 h at 37°C counted every 24 h (n = 3 independent experiments with at least 429 animals/experiment).

C Per cent survival of wild-type animals fed with bacteria expressing either control or the indicated RNAi construct diluted 1:1 following paraquat (8 mM) administration and counted every 24 h (n = 3 independent experiments with at least 603 animals/experiment).

D Per cent survival of wild-type animals fed with bacteria expressing either control or the indicated RNAi construct diluted 1:1 and subjected to heat stress for 5 h at 37°C counted every 24 h (n = 3 independent experiments with at least 603 animals/experiment).

Data information: Error bars denote SEM. Stress assays were performed at 20°C; detailed data are given in Tables EV1–EV3.

© 2023 The Authors

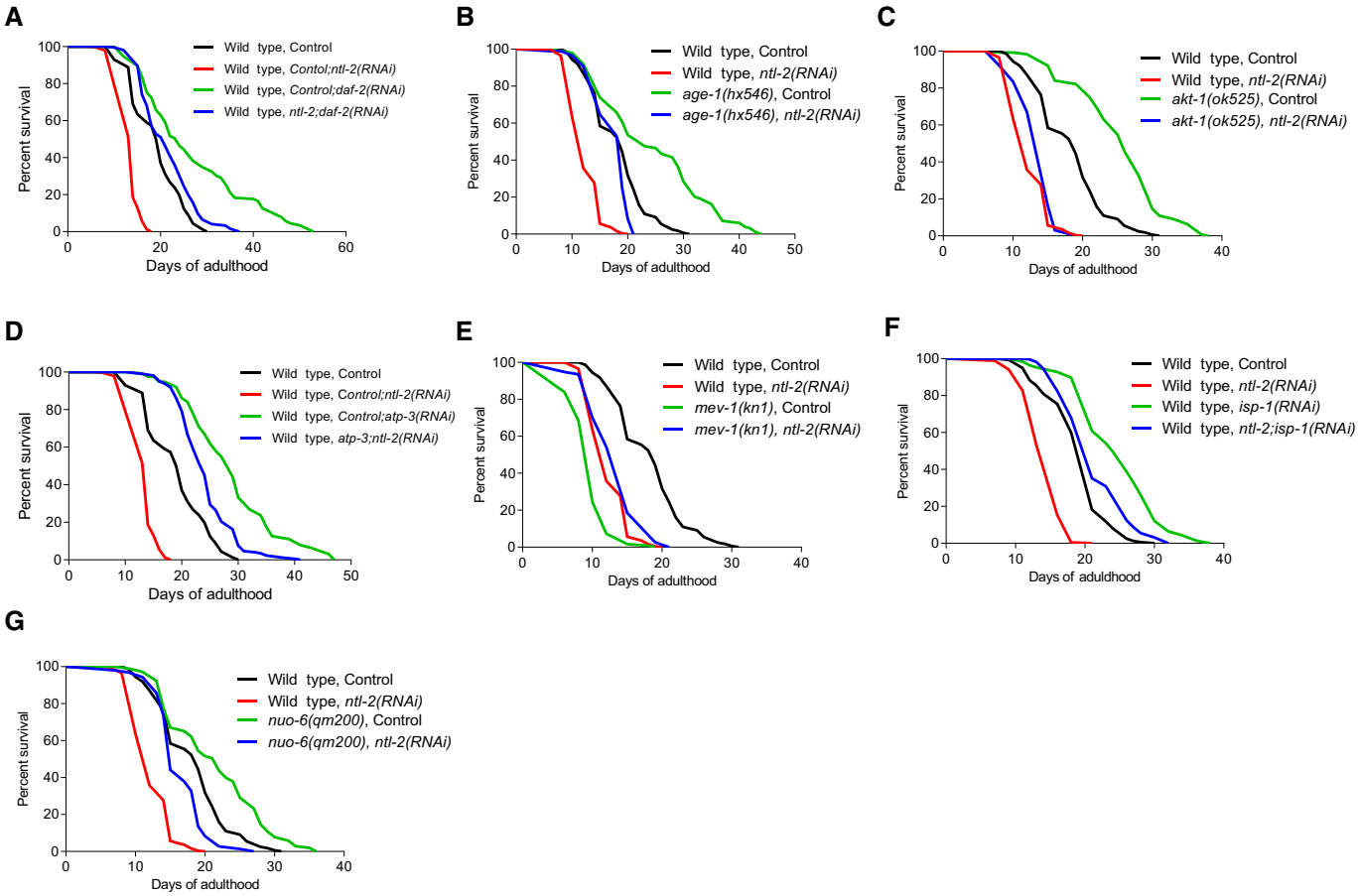

Figure EV5. Genetic inhibition of *ntl-2* shortens the lifespan of long-lived insulin/IGF-1 pathway mutants and differentially impacts longevity of animals with compromised mitochondrial function.

A Knockdown of *ntl-2* shortens the lifespan of *daf-2(RNAi)* long-lived animals.
B Knockdown of *ntl-2* shortens the lifespan of *age-1(hx546)* mutants.
C Knockdown of *ntl-2* shortens the lifespan of *akt-1(ok525)* mutants.
D Knockdown of *atp-3 rescues* the short lifespan of NTL-2-depleted animals.
E *mev-1(kn1)* mutation is beneficial for the lifespan of NTL-2-depleted animals.
F Knockdown of *isp-1* rescues the short lifespan of NTL-2-depleted animals.
G *nuo-6(qm200)* mutation is beneficial for the lifespan of NTL-2-depleted animals.

Data information: Lifespan assays were performed at 20°C; detailed data are given in Table EV4.

© 2023 The Authors